Electronic Supplementary Material (ESI) for Chemical Communications.

Novel $LiV(PO_4)_{0.9}F_{1.3}$ with ultrahigh rate capability and prolonged cycle life

Meichen Zhang,[a] Yongmao Zhou,[a] Xiaobo Ding,[a] Guochun Yan,[a] and Jiexi Wang [a,b,*]

[a] School of Metallurgy and Environment, Central South University, Changsha 410083, P. R. China

[b] State Key Laboratory for Powder Metallurgy, Central South University, Changsha 410083, P. R. China

* Corresponding author, email address: wangjiexikeen@csu.edu.cn

Experimental

1 Material preparation

$LiV(PO_4)_{1-x}F_{1+3x}$ (x=0-0.2 with the interval of 0.025 between each point) samples were prepared by solid-state method with mechanical activation as introduced in our previous work.[1, 2] At first, V_2O_5 (AR, 99%), LiF (Macklin, 99.9%), PVDF (9300, Cell Grade, Kureha), $NH_4H_2PO_4$ (Sigma-Aldrich, 99.5%), $H_2C_2O_4 \cdot 2H_2O$ (Macklin, 99.5%) were mixed with 50 mL alcohol. Then, the obtained suspension was ball-milled at 400 r min^{-1} for 8 h. After that, the mixture was dried at 120 ^oC for 15 h. Finally, the powder was pre-sintered at 350 ^oC for 5h and pelletized at 650 ^oC for 2 h under argon with 5 ^oC min^{-1}.

2 Material characterization

The chemical composition of all the samples was measured via inductive coupled plasma (ICP, Spectro Blue Sop). The valence of the elements was tested by the X-ray photoelectron spectroscopy (XPS, K-ALPHA). X-ray diffractometer (TTR III) and Rietveld refinement software (GSAS) were employed in a range of 10~80° to analyze the crystallographic structure and phase composition of the samples. The electronic conductivities of samples were tested by the semiconductor powder resistivity tester (ST-2722). Scanning electron microscope (SEM, Nova Nano 230) and aberration corrected scanning transmission electron microscopy (TEM, G260-300) were used to characterize the particle size and micro-morphologies of the samples.

3 Electrochemical tests

The electrochemical properties of synthesized cathode materials were tested via using CR2025 coin cell. The active material, conductive carbon (*Keqin black*) and polyvinylidene fluoride with a weight ratio of 8:1:1 were fully ground and mixed in N-methyl pyrrolidinone. Then the obtained slurry was evenly coated on a carbon-coated Al foil and dried at 120 ^oC for 3 hours. The dried cathode sheet was cut into 7 mm radius wafers, and then dried at 60 ^oC for 8 hours in a vacuum oven. CR2025 coin-type cells composed of as-fabricated working electrode, lithium foil counter electrode, separator (Celgard 2300) and electrolyte (1 mol L^{-1} $LiPF_6$ in EC/DEC) were assembled into in a dry Ar-filled glove box. Galvanostatic tests were carried out on a

NEWARE charge-discharge tester at the range of 2.5-4.5 V at specific rates (1 C = 156 mAh g^{-1}). The electrochemical impedance spectroscopy tests (EIS) were carried on CHI660A workstation by applying an AC voltage of 5 mV amplitude in the frequency range of 0.01 Hz–100 kHz. The galvanostatic intermittent titration technique (GITT) measurement was programmed by supplying a constant discharge current flux of 0.1 C for 10 min followed by an open circuit stand for 50 min, respectively, from 4.5 to 2.5 V.

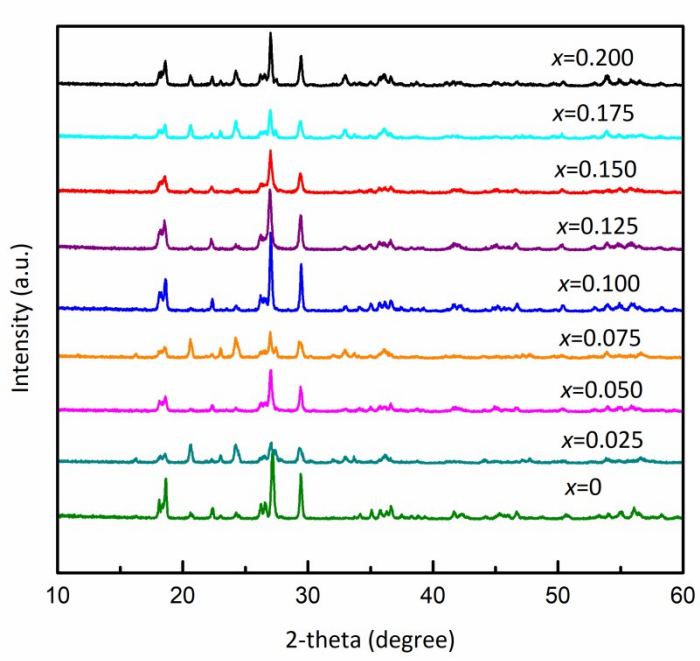

Figure S1 XRD patterns of $LiV(PO_4)_{1-x}F_{1+3x}$ (x=0-0.2) with sweep velocity of 10° min^{-1}

Table S1 ICP analysis of elemental ratio for $LiV(PO_4)_{0.9}F_{1.3}$ and $LiVPO_4F$

Sample	Theoretical proportion Li:V:P	Actual proportion Li:V:P
$LiV(PO_4)_{0.9}F_{1.3}$ precursor	1:1:0.9	0.9986:1:0.8985
$LiV(PO_4)_{0.9}F_{1.3}$	1:1:0.9	0.9953:1:0.8913
$LiVPO_4F$	1:1:1	0.9894:1:0.9951

The ratio of element Li, V and P in $LiV(PO_4)_{0.9}F_{1.3}$ and $LiVPO_4F$ was figured out using ICP. Related data are listed in Tab.1. The elemental ratio of as-synthesized

samples is quite close to the planned stoichiometric ratios. And compared with element V, the content of element Li and P of materials were a little lower than planned ratio. The results show clearly that both lithium and phosphorus would be easier to evaporate and lose than vanadium during heating process. Further comparative analysis of the elemental ratios in precursor and sintered products of $LiV(PO_4)_{0.9}F_{1.3}$. The loss of elements in ball-milling process is less than that in sintering process.

Table S2 Atomic positions of the $LiV(PO_4)_{0.9}F_{1.3}$ sample obtained from the Rietveld refinement results (Number of formula units, Z: 2)

Site	*x/a*	*y/b*	*z/c*	Occupation
V1	0.0	0.0	0.0	1
V2	0.5	0.5	0.5	1
P1	0.5711422	0.89391917	0.24690872	1
O1	0.6722822	0.7046666	0.35957196	1
O2	0.6686913	0.19518264	0.4035377	1
O3	0.7182576	0.8525103	0.08918483	1
O4	0.25388405	0.81895626	0.14382249	1
F1	0.1427187	0.34126908	0.25113043	1
Li1	0.8451456	0.54759693	0.18	1
Li2	0.0116768	0.6055202	0.25	1

Table S3 Atomic positions of the $LiVPO_4F$ sample obtained from the Rietveld refinement results (Number of formula units, Z: 2)

Site	*x/a*	*y/b*	*z/c*	Occupation
V1	0.0	0.0	0.0	1
V2	0.5	0.5	0./5	1
P1	0.5650241	0.8956502	0.23830691	1
O1	0.6668624	0.7024947	0.3652129	1
O2	0.64214647	0.19504775	0.38407728	1
O3	0.7009323	0.86494684	0.08181963	1
O4	0.25977063	0.84859025	0.15848935	1
F1	0.15983771	0.33617598	0.25673	1
Li1	0.73792535	0.3296785	0.13191012	1
Li2	0.00058603205	0.632888	0.25	1

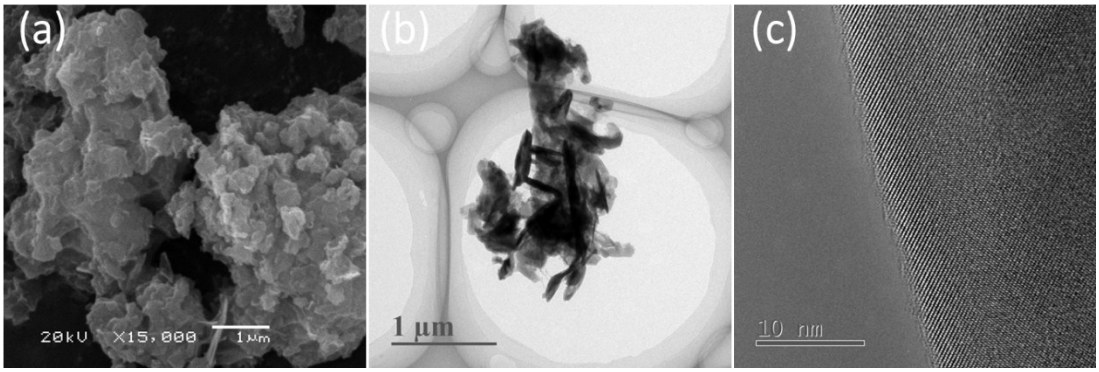

Figure S2 Morphology and elemental distribution of $LiVPO_4F$ sample: (a) SEM images; (b) TEM images; (c) HRTEM images.

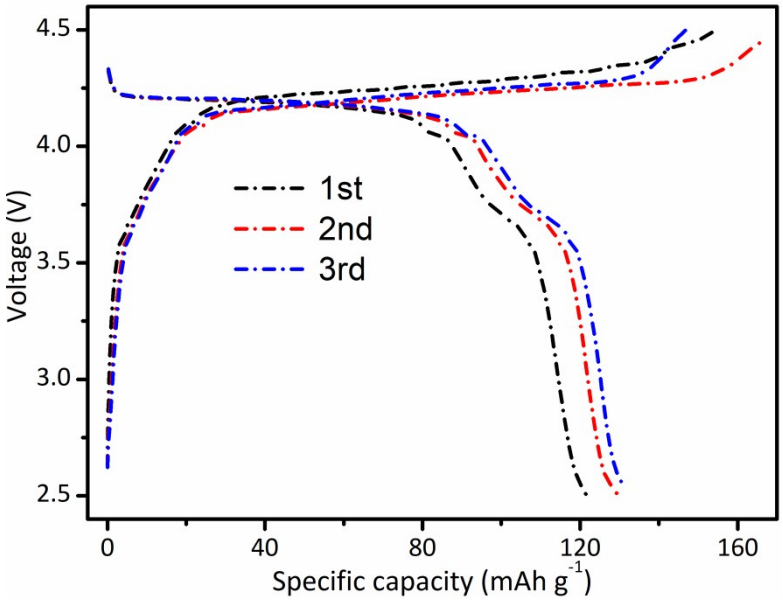

Figure S3 Initial three charge-discharge profiles of $LiVPO_4F$ sample at 0.2 C in the voltage range of 2.5-4.5 V

The redox reactions of $LiV(PO_4)_{0.9}F_{1.3}$ are shown as follows:

$$LiV^{\mathrm{III}}(PO_4)_{0.9}F_{1.3} - xLi^+ - xe^- \overset{Charging}{\rightarrow} Li_{1-x}(V^{\mathrm{IV}})_x(V^{\mathrm{III}})_{1-x}(PO_4)_{0.9}F_{1.3} \quad \text{Equation S1}$$

$$Li_{1-x}(V^{\mathrm{IV}})_x(V^{\mathrm{III}})_{1-x}(PO_4)_{0.9}F_{1.3} + xLi^+ + xe^- \overset{Discharging}{\rightarrow} LiV^{\mathrm{III}}(PO_4)_{0.9}F_{1.3} \quad \text{Equation S2}$$

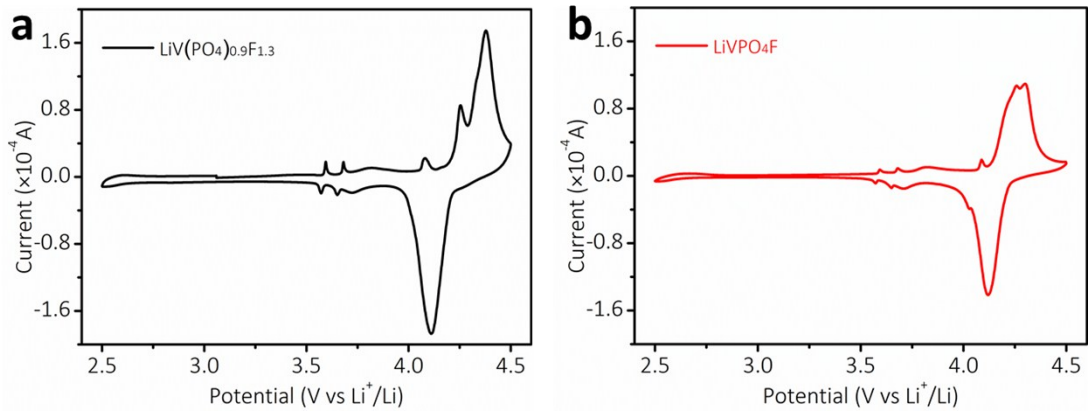

Figure S4 The cyclic voltammetry curves of (a) $LiV(PO_4)_{0.9}F_{1.3}$ and (b) $LiVPO_4F$ in Li half cells (the scanning speed is 0.1 mV s^{-1}).

Cyclic voltammetry curves of $LiV(PO_4)_{0.9}F_{1.3}$ (Figure S4a) possesses two main oxidation peaks (corresponding to the two-steps of potential at 4.25 V and 4.2V in

Figure 3a), which originates from the intermediate phase ($Li_{0.67}VPO_4F$) during the charging process of LVPF. Three redox peaks below 4.2 V are indexed with typical Li^+ (de)intercalation behavior in $Li_3V_2(PO_4)_3$ lattices following $Li_3V_2(PO_4)_3 \xrightarrow{3.6\ V} Li_{2.5}V_2(PO_4)_3 \xrightarrow{3.7\ V} Li_2V_2(PO_4)_3 \xrightarrow{4.1\ V} LiV_2(PO_4)_3$, verifying the presence of $Li_3V_2(PO_4)_3$ impurity as demonstrated in the XRD pattern (Figure S1). The related redox reactions of $Li_3V_2(PO_4)_3$ impurity are shown in Equation (3-5):

$$Li_3V_2(PO_4)_3 - 0.5Li^+ - 0.5e^- \leftrightarrow Li_{2.5}V_2(PO_4)_3 \quad \text{Equation (3)}$$

$$Li_{2.5}V_2(PO_4)_3 - 0.5Li^+ - 0.5e^- \leftrightarrow Li_2V_2(PO_4)_3 \quad \text{Equation (4)}$$

$$Li_2V_2(PO_4)_3 - Li^+ - e^- \leftrightarrow LiV_2(PO_4)_3 \quad \text{Equation (5)}$$

The redox peaks of $LiV(PO_4)_{0.9}F_{1.3}$ are steeper and sharper than that of $LiVPO_4F$, which indicates that $LiV(PO_4)_{0.9}F_{1.3}$ achieves higher energy density and the speed of (de)intercalation of Li^+ ions in $LiV(PO_4)_{0.9}F_{1.3}$ has been enhanced to a certain extent.

Table S4 The comparison for performance of as-prepared $LiV(PO_4)_{0.9}F_{1.3}$ with that of state-of-the-art lithium vanadium fluophosphates

Sample	Discharge capacity (mAh g^{-1})									Ref.
	0.1C	0.2C	1C	5C	10C	20C	40C	50C	60C	
$LiV(PO_4)_{0.9}F_{1.3}$	**--**	**156**	**146**	**--**	**137**	**127**	**--**	**105**	**--**	**This work**
$LiVPO_4F$/N-doped graphene	153	152	144	132	123	104	--	--	--	[3]
$LiVPO_4F$/C-PVDF	148	--	145	136	--	--	--	--	--	[4]
$LiVPO_4F$@C- sol-gel	148	--	136	121	--	--	--	--	--	[5]
$Li_{0.99}K_{0.01}VPO_4F$	141[a]	--	133	--	98	--	--	--	--	[6]
Ag-coated $LiVPO_4F$	--	117	104	82	--	--	--	--	--	[7]
$LiVPO_4F$/C-PTFE	142	--	136	--	120	130[b]	120[b]	--	102[b]	[8]
$Li_{0.99}K_{0.01}V_{0.995}Zr_{0.005}PO_4F$/C	143	--	136	--	108	119[b]	110[b]	--	106[b]	[9]
$LiVPO_4F$ nanosheets	143	--	125	104	--	--	--	--	--	[10]

Note: [a] This data was obtained at 0.12C; [b] These data were obtained by charging at 1C.

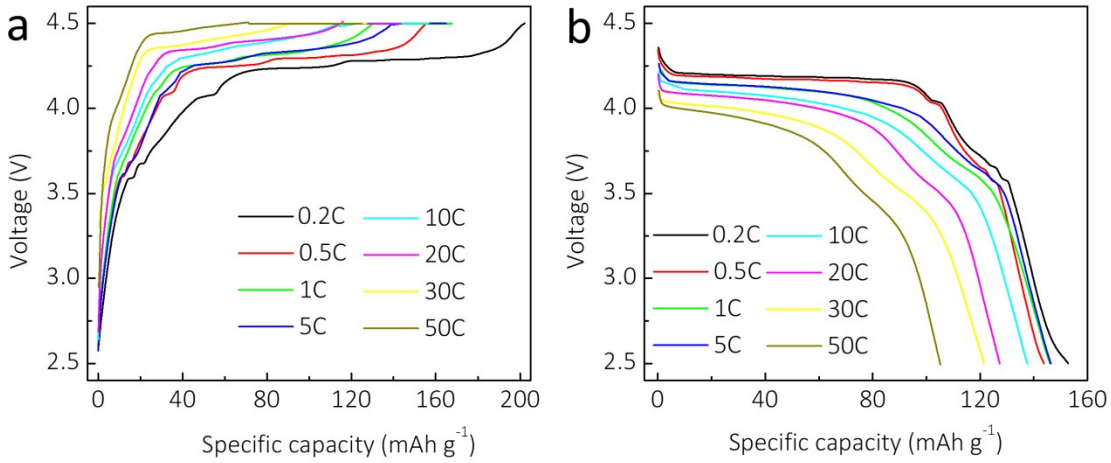

Figure S5 (a) Charge and (b) discharge profiles of $LiV(PO_4)_{0.9}F_{1.3}$ sample at various C-rates ranging from 0.2 C to 50 C.

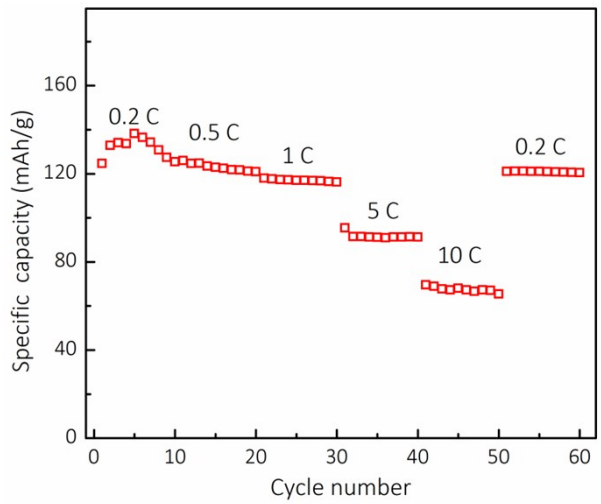

Figure S6 Rate capability of $LiVPO_4F$ sample from 0.2 C to 10 C

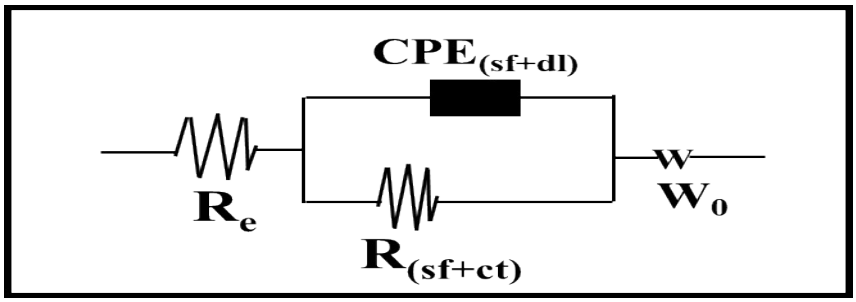

Figure S7 Equivalent circuit model employed for fitting the obtained EIS data

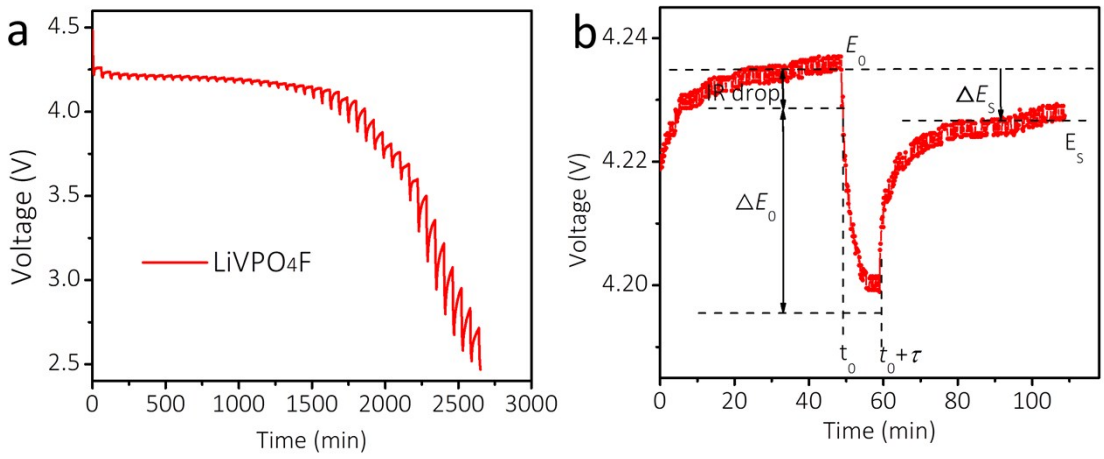

Figure S8 (a) GITT full curve and (b) typical single GITT titration curve of $LiVPO_4F$ sample

References

1. J. Wang, Z. Wang, X. Li, H. Guo, X. Wu, X. Zhang and W. Xiao, *Electrochimica Acta*, 2013, **87**, 224-229.
2. J. Wang, X. Li, Z. Wang, B. Huang, Z. Wang and H. Guo, *Journal of Power Sources*, 2014, **251**, 325-330.
3. K. Cui, S. Hu and Y. Li, *Journal of Power Sources*, 2016, **325**, 465-473.
4. W.-h. Zhang, T. Luo, C.-l. Fan, Q.-y. Li, K. Shi, L.-f. Li, T.-t. Zeng, Z. Wen, S.-c. Han and J.-s. Liu, *Journal of Alloys and Compounds*, 2019, **778**, 345-358.
5. Y. Shi, J. Luo, R. Wang, J. Zhao and Q. Xie, *Solid State Ionics*, 2018, **327**, 71-75.
6. J. Wu, Y. Xu, X. Sun, C. Wang, B. Zhang and J. Zhao, *Journal of Power Sources*, 2018, **396**, 155-163.
7. B. Yang and L. Yang, *Journal of Physics and Chemistry of Solids*, 2015, **87**, 228-232.
8. M. Kim, S. Lee and B. Kang, *Advanced Science*, 2016, **3**, 1500366.
9. J. Wu, Y. Xu, Y. Chen, L. Li, H. Wang and J. Zhao, *Journal of Power Sources*, 2018, **401**, 142-148.
10. B. Zhang, Y.-d. Han, J.-c. Zheng, C. Shen, L. Ming and J.-f. Zhang, *Journal of Power Sources*, 2014, **264**, 123-127.